MS accepted by *J. Anim. Ecol.*

Moving on with foraging theory: incorporating movement decisions into the functional response of a gregarious shorebird

Jan A. van Gils[1*], Matthijs van der Geest[1], Brecht De Meulenaer[1], Hanneke Gillis[1], Theunis Piersma[1,2], and Eelke O. Folmer[1]

[1]*Department of Marine Ecology, NIOZ Royal Netherlands Institute for Sea Research, P.O. Box 59, 1790 AB Den Burg (Texel), The Netherlands; and* [2]*Chair in Global Flyway Ecology, Animal Ecology Group, Centre for Ecological and Evolutionary Studies (CEES), University of Groningen, P.O. Box 11103, 9700 CC Groningen, The Netherlands*

*Correspondence author. E-mail: Jan.van.Gils@nioz.nl

Summary

1. Models relating intake rate to food abundance and competitor densities (generalized functional response models) can predict forager distributions and movements between patches, but we lack understanding of how distributions and small-scale movements by the foragers themselves affect intake rates.

2. Using a state-of-the-art approach based on continuous-time Markov chain dynamics, we add realism to classic functional response models by acknowledging that the chances to encounter food and competitors are influenced by movement decisions, and, vice versa, that movement decisions are influenced by these encounters.

3. We used a multi-state modelling framework to construct a stochastic functional response model in which foragers alternate between three behavioural states: searching, handling and moving.

4. Using behavioural observations on a molluscivore migrant shorebird (red knot, *Calidris canutus canutus*), at its main wintering area (Banc d'Arguin, Mauritania), we estimated transition rates between foraging states as a function of conspecific densities and densities of the two main bivalve prey.

5. Intake rate decreased with conspecific density. This interference effect was not due to decreased searching efficiency, but resulted from time lost to avoidance movements.

6. Red knots showed a strong functional response to one prey (*Dosinia isocardia*), but a weak response to the other prey (*Loripes lucinalis*). This corroborates predictions from a recently developed optimal diet model that accounts for the mildly toxic effects due to consuming *Loripes*.

7. Using model-averaging across the most plausible multi-state models, the fully parameterized functional response model was then used to predict intake rate for an independent dataset on habitat choice by red knot.

8. Comparison of the sites selected by red knots with random sampling sites showed that the birds fed at sites with higher than average *Loripes* and *Dosinia* densities, i.e. sites for which we predicted higher than average intake rates.

9. We discuss the limitations of Holling's classical functional response model that ignores movement and the limitations of contemporary movement ecological theory ignoring consumer-resource interactions. With the rapid advancement of technologies to track movements of individual foragers at fine spatial scales, the time seems ripe to integrate descriptive tracking studies with stochastic movement-based functional response models.

Key-words: competition, continuous-time Markov chain, cryptic interference, diet, distribution, habitat choice, movement ecology, intake rate, predation, toxic prey

Introduction

Fine-scale spatial movements of foragers are steered by encounters with food items, the presence of competitors, and by the social benefits of living in a group. There is a growing body of literature on how the attractant forces of food interact with the opposing forces of conspecific attraction and repulsion (e.g. Folmer, Olff & Piersma 2010). Movement ecology is the emerging field in which these processes come together (Nathan *et al.* 2008). To make progress, we need a good understanding of what determines a forager's encounter rate with both its group members and its prey (Gurarie & Ovaskainen 2013). Functional response models link foragers to their prey and other foragers (Jeschke, Kopp & Tollrian 2002) and are a good starting point for modelling socially- and food-mediated movements (Avgar, Kuefler & Fryxell 2011).

In a substantial number of functional response models, the effects of prey density have been integrated with the effects of competitor density (i.e. the so-called 'generalized functional responses' reviewed by van der Meer & Ens 1997). As stressed by van der Meer & Ens (1997), most of these models are phenomenological because they lack a mechanistic underpinning of the processes of prey and competitor encounter, rendering it difficult to use them as firm building blocks in follow-up studies. Unfortunately, ratio-dependent predation models, which have been claimed to offer an altered perspective on trophic ecology (Arditi & Ginzburg 2012), are of phenomenological nature too (Abrams 2014). But note that even the few generalized functional response models that do mechanistically include competition have significant drawbacks. Most importantly, these models are built on the assumption that agonistic interactions are inevitable when two foragers meet. This rigid approach excludes the realistic possibility that foragers could avoid agonistic conflict situations by moving away from each other (Folmer, Olff & Piersma 2012). Recent empirical work has shown that socially foraging red knots (*Calidris canutus*) indeed avoid agonistic interactions (Bijleveld, Folmer & Piersma 2012). The time cost associated with this avoidance behaviour has been labelled 'cryptic interference' (Gyimesi, Stillman & Nolet 2010; Bijleveld, Folmer & Piersma 2012). Not unexpectedly, the few models that include

avoidance behaviour do a better job in explaining variations in intake rate than models that ignore avoidance (Stillman, Goss-Custard & Caldow 1997; Stillman *et al.* 2000). However, in such models foragers only move for reasons of competition, while there are other reasons to change location.

Among these reasons are the benefits of staying in the vicinity of group members, that may provide shelter (Wiersma & Piersma 1994), safety (Elgar 1989) and information (Couzin *et al.* 2005). Such benefits might indirectly affect food intake rates (Beauchamp 1998). For example, under experimental conditions in which the possibility for physical interference was eliminated, starlings (*Sturnus vulgaris*) feeding close together showed enhanced food intake and foraging efficiency compared with birds feeding further apart (Fernández-Juricic, Siller & Kacelnik 2004). Efforts to embed socially-mediated behaviour into functional response models are still at their infancy (Folmer, Olff & Piersma 2012). Not surprisingly, such models are yet to be developed and tested in the natural world.

The ways in which the presence (or absence) of food determines forager movements have been studied across wide range of organisms and spatial scales (e.g. Fryxell *et al.* 2008; Owen-Smith, Fryxell & Merrill 2010). Within contemporary movement ecology, there is much attention for how foragers should and do move through landscapes in search of food patches (Sims *et al.* 2008). Once in a patch and having encountered prey, it pays a forager to continue searching where it last found a prey (van Gils 2010), a strategy called ‘area-restricted search’ (Tinbergen, Impekoven & Franck 1967). Recently, there have been theoretical efforts to enforce the link between prey taxis to consumption rates (Chakraborty *et al.* 2007; Avgar, Kuefler & Fryxell 2011), but these studies have not yet received empirical scrutiny.

In this paper we integrate food- and the socially-driven aspects of movement into an empirically-derived functional response model by means of continuous-time Markov chain modelling. This modelling approach allows the construction of realistic functional response models by explicitly taking into account the fact that finding food and running into competitors are sequential and stochastic events. In such models, foragers can alternate between behavioural states at any moment in time (hence 'continuous time';

van der Meer & Smallegange 2009), in which the instantaneous risk of switching to another state has 'Markov property', i.e. transition rates depend only on the present behavioural state. Software to estimate statistical 'multi-state models' is available (e.g. Jackson 2011), which enables empirical analysis of transition rates between behavioural states as a function of food availability and the presence of group members (Smallegange & van der Meer 2010).

We develop realistic functional response models for the well-studied red knot (Piersma & van Gils 2011; Piersma 2012) on the basis of observed foraging behaviour. These models are then used to predict spatial distributions on the basis of its food distributions. We start off by constructing a Markov chain functional response model in which foragers alternate between the behavioural states "searching for food", "handling food", and "moving without searching". Next, we fit this model to focal sampling data collected on 1,242 individual free-ranging red knots at their main wintering area in Banc d'Arguin (Mauritania), in which transition rates between searching, handling and moving are related to prey and conspecific densities. The best models are then used to make spatially explicit predictions on (interference-free) intake rate with an independent dataset on food abundance, collected in another year. The predictive power of the models is investigated by relating the exact positions of 5,666 individual red knots to predicted (interference-free) intake rates.

CONTINUOUS-TIME MULTI-STATE MARKOV CHAIN MODEL

In the model, graphically depicted in Fig. 1, a forager can be in three mutually exclusive behavioural states (handling H, searching S and moving M), with five possible transitions between these states. From the searching state, a forager can either switch to the handling or the moving state. The rate at which a searching forager 'switches' to the handling state is better known as prey encounter rate and is symbolized in our model by β. The rate at which a searching forager decides to move on is given by δ. Thus, the total rate of a searching forager to stop searching, either due to a prey encounter or a decision to

121 move on, is given by β + δ. The inverse of this sum is the average length of a search bout. The rate at
122 which a handling forager switches back to the searching state is given by α, while the rate of switching to
123 the moving state is given by μ. Finally, a moving forager can only go back to the searching state and the
124 rate at which this occurs is given by γ. A moving forager cannot find a prey and hence transitions from
125 moving to handling do not exist.

126 The following set of differential equations describes the dynamics in the number of handling (*H*),
127 searching (*S*) and moving (*M*) foragers:

128 $$\frac{dH}{dt} = \beta S - \alpha H - \mu H \quad \text{eqn 1}$$

129 $$\frac{dS}{dt} = \alpha H - \beta S + \gamma M - \delta S \quad \text{eqn 2}$$

130 $$\frac{dM}{dt} = \delta S - \gamma M + \mu H \quad \text{eqn 3}$$

131 At equilibrium, the number of individuals in each state is constant, which implies that each differential
132 equation can be set to zero. This allows the equilibria *H**, *S** and *M** to be calculated:

133 $$H^* = \frac{\beta S^*}{\alpha+\mu} \quad \text{eqn 4}$$

134 $$S^* = \frac{\alpha H^* + \gamma M^*}{\beta+\delta} \quad \text{eqn 5}$$

135 $$M^* = \frac{\delta S^* + \mu H^*}{\gamma} \quad \text{eqn 6}$$

136 Since the total number *F** of foragers can be expressed as *F** = *H** + *S** + *M**, the proportion of birds in
137 the searching state at equilibrium can be written as (after substituting eqn 4 for *H** in eqn 6):

138 $$\frac{S^*}{F^*} = \frac{(\alpha+\mu)\gamma}{(\alpha+\beta+\mu)\gamma+(\alpha+\mu)\delta+\mu\beta} \quad \text{eqn 7}$$

139 The multiplication of $\frac{S^*}{F^*}$ with the transition rate β from searching to handling (i.e. the encounter rate with
140 prey while searching), gives the per capita intake rate (van der Meer & Smallegange 2009). In the
141 STATISTICS section below we explain how we linked covariates to transition rates.

142

143 ## Materials and methods

144 All data were collected in the Parc National du Banc d'Arguin, around the small fishery village of Iwik
145 (Fig. 2A; Leyrer *et al.* 2012; van den Hout *et al.* 2014). To develop the multi-state functional response
146 models and to test how well they predict foraging distributions, data on intake rate and on foraging
147 distributions were collected during two separate expeditions. Behavioural data, which formed the basis
148 for the Markov chain modelling, were collected in January-February 2008. Spatial distributions were
149 collected between March and April 2007. Prey densities were sampled in both years.

150

151 ### INTAKE RATE PROTOCOLS (2008)

152 Observations on intake rates were carried out at three different sites in our study area (Fig. 2A). We
153 returned to each site every third day to carry out observations. At two sites (site D and I) the observers sat
154 on top of an aluminium scaffolding tower (LWH = 2×1×2 m), at the other site (site A) observations were
155 carried out from a nearby dune. In total, 5 days were spent at site A (covering 7 low-tide periods), 5 days
156 at site D (5 low-tide periods), and 6 days at site I (6 low-tide periods). In total, we carried out
157 observations on 1,242 individual birds (411 at site A; 324 at site D; 507 at site I).

158 Using 20-60×spotting scopes, we applied focal sampling by selecting focal individuals
159 haphazardly. Each protocol comprised the period between two consecutive prey captures (mean ± SD
160 duration = 39.0 ± 42.0 s). During this interval, behaviour was recorded using a voice-recorder (Philips

Digital Voice Tracer 7655) and was categorized into 9 different classes (searching, handling, walking, looking up, preening, chasing or being chased, flying, washing, drinking). Recorded observations were digitized using the freeware package EthoLog (Ottoni 2000). To avoid unwieldy models, we only considered transitions between the 3 most frequent behaviours (searching, handling and moving), and excluded transitions between the other 6 behaviours (which together made up only 6% of the total time budget). Using numbered wooden sticks, we divided an annulus (outer radius 200 m, inner radius 100 m) around the observation tower into 128 equally sized 'bird sections' (Fig. 2B). At site A the observational arena comprised half an annulus (outer radius 100 m, inner radius 50 m), which was divided into 20 sections. The section in which the focal bird fed, together with the estimated distance from tower, enabled us to determine the position of the focal bird, which was used to assign a prey density estimate to each observation (see below). The total number of red knots, including the focal bird, present in the focal bird's section was counted immediately after the protocol ended, which was used as our measure of knot density. Before the analysis, the number of red knots per plot at site A (589 m^2/plot) was multiplied by 1.25 to make them comparable to the densities at the other two sites (736 m^2/plot). All observations were carried out by JAvG and HG. To prevent possible observer bias, both observers carried out simultaneous observations on the same birds during the two days preceding data collection.

RED KNOT DISTRIBUTION (2007)

In 2007 we mapped the positions of individual red knots on 7 different tidal flats in our study area (sites B-H; Fig. 2A), spending a single day at each site (usually covering a single low tide period, but sometimes two half low tide periods). Again we worked from a single scaffolding tower, which we relocated between observation days. As described above, an observation area comprised an annulus around the tower (outer radius 200 m, inner radius 100 m), with the annulus split up into 128 equally sized and shaped parts using poles placed at known coordinates (Fig. 2B).

185 Every half hour a photo was taken of each section, using a DSLR-camera (6.1 MP) with a 300-
186 mm lens and 1.4 teleconvertor attached to it. Using this setup, one bird section fitted exactly into one
187 photograph, while allowing recognition of individual bird species. With 64 half hours across all 7 sites we
188 obtained a total of 8,192 photos. The photographs were loaded into a GIS where the poles (indicating the
189 section corners) and all individual birds were marked and given relative coordinates. The points
190 describing the locations of the poles and birds were stored in a vector file. As the poles' geographical and
191 relative coordinates were known, we were able to calculate the birds' geographical coordinates on the
192 basis of principles of projective geometry for which we used Matlab R2011a. We first calculated the
193 parameters of the projective transformation on the basis of the poles' relative and geographical
194 coordinates. Then the projection parameters were used to project the birds' relative positions to
195 geographical coordinates. In total, we calculated the positions of 5,666 individual red knots in this way.

196

197 PREY DENSITY AND INTERPOLATION

198 In both years, prey densities were estimated by taking sediment core samples at a number of stations
199 inside the annulus around each tower. We divided the annulus around each tower into 16 equally sized
200 'benthos sections' where benthos was sampled (the half annulus at site A used in 2008 was divided into
201 three 'benthos sections'). In each benthos section we randomly selected two locations (Fig. 2B). At each
202 location two cores were taken. The distance between the cores at one location was 1 m in a random
203 direction (to the benefit of estimating the autocorrelation function at short distances required for kriging,
204 see below). In total we collected 448 benthos samples in 2007 ($7 \times 16 \times 2 \times 2$) and 140 samples in 2008
205 ($2 \times 16 \times 2 \times 2 + 1 \times 3 \times 2 \times 2$).

206 Following procedures published elsewhere (van Gils *et al.* 2013), samples were taken with a
207 sediment core with a diameter of 15 cm to a depth of 20 cm. To distinguish prey that were accessible to
208 red knots from those that were not, we separated the top (0-4 cm) from the bottom layer (4-20 cm; red

knots have bills of 3.5-4.0 cm length) and sieved both layers over a 1-mm mesh. In the laboratory samples were sorted and each specimen was identified to species or genus level. Lengths were determined to the nearest 0.1 mm. As just two prey species at Banc d'Arguin dominate the food supply and diet of red knot (van Gils *et al.* 2012; Onrust *et al.* 2013; van Gils *et al.* 2013; van den Hout *et al.* 2014), we included only these two species in the analyses (*Dosinia isocardia*; *Loripes lucinalis*). *Dosinia* larger than 13.2 mm long were excluded from the analyses as red knots ingest their prey whole and are therefore gape-width limited in their diet choice (Zwarts & Blomert 1992).

To estimate available *Loripes* and *Dosinia* densities at the individual bird positions (be it a focal bird in the intake rate protocols or a 'photo bird' in the 2007 distributional analysis), the sampled densities were interpolated by means of universal kriging. Because seagrass cover correlates with both *Loripes* and *Dosinia* density (Honkoop *et al.* 2008; van der Heide *et al.* 2012), and because NDVI (Normalized Difference Vegetation Index) is a good proxy for seagrass coverage in our study area (Folmer *et al.* 2012), we used NDVI and $NDVI^2$ as auxiliary predictors of prey density. NDVI was derived from an image taken on 21 August 2007 at 11:25 AM GMT by the Landsat 5 TM satellite (the date most intermediate to both expeditions). The image was taken 1:25 h before local low tide (using the Dakar tidal chart and assuming a 5 hour delay in Iwik; Wolff & Smit 1990), with an average cloud cover of 10% (but being 0% for our study area). Following standard procedures (Kriegler *et al.* 1969), NDVI was calculated as $\frac{\text{NIR-red}}{\text{NIR+red}}$, with the NIR reflection given by band 4 and the red reflection given by band 3 (both at a 30 by 30 m resolution; Fig. 2).

The best regression models for the deterministic parts of universal kriging were obtained as follows. Prey densities were $\log_e$-transformed to normalize the distributions. We added 1 to the arguments to avoid taking the logarithm of zero (which we subtracted after back-transforming the interpolated densities). We estimated the full model which included NDVI and $NDVI^2$ as predictors and the nested sub-models (i.e. only NDVI or $NDVI^2$ as a predictor). For the deterministic part in universal kriging we

used the model with the lowest AIC value (results are given in Table S1 in Supporting Information). For kriging we used the R package *automap* (Hiemstra *et al.* 2008), which builds on package *gstat* (Pebesma 2004) and enables automatic interpolation. In this way, the regression- and geostatistical models may differ between tidal flats.

STATISTICS

Multi-state models were fitted with R (R Core Team 2013) using the *msm* package (Jackson 2011), which enables multi-state models to be fitted to longitudinal data (i.e. observations of state collected on the same subjects at multiple points in time). The *msm* package is able to estimate transition rates without knowing the exact moments of state changes; however, in our case we knew these exact moments, which obviously improves the accuracy of estimating transition rates. We explored how these rates covaried with available *Dosinia* density, available *Loripes* density, summed density of available *Dosinia* and *Loripes* together, and red knot density, testing for all possible combinations and interactions (but excluding combinations of summed prey density on the one hand and *Dosinia* or *Loripes* density on the other hand, since summed prey density is the sum of *Dosinia* and *Loripes* density). In the *msm* package these effects were tested using the proportional hazard model (Marshall & Jones 1995) as expressed below, taking transition rate β from searching to handling as an example:

$$\beta_i = \beta_{0,i} \exp\left(b_1 X_{1,i} + b_2 X_{2,i} + \cdots + b_k X_{k,i}\right) \quad \text{eqn 8}$$

In this model, β_i is the transition rate β of observation i on an individual's searching state, $\beta_{0,i}$ is this observation's baseline transition rate (i.e. $\beta_i = \beta_{0,i}$ when covariates set to 0), $X_{1,i}...X_{k,i}$ are k covariates and $b_1...b_k$ their statistical effects (note that the model has the same structure for transition rates α, γ, δ and μ). The model is proportional in the sense that effects of the covariates are multiplicative with respect to baseline rates (e.g. each unit increase in covariate X_1 would result in a proportional scaling of transition

rate β). Further note that Markov models require individual bout lengths (i.e. the inverse of transition rate) to be exponentially distributed; a requirement for which we tested using the Cramér-von Mises test (using R package exptest; Pusev & Yakovlev 2011). Models were selected on the basis of Akaike's Information Criterion (AIC; Burnham & Anderson 2002). Particularly, all models were ranked in order of increasing AIC values; with the model showing the lowest AIC value considered as the best model. Following Burnham & Anderson (2002), models with $\Delta AIC < 2$ relative to the best model were also considered. All models were included for model-averaging (including those with $\Delta AIC \geq 2$), using each model's AIC weight as a weighing factor.

We used bagplots to explore the spatial distribution of red knots in relation to prey densities (using the aplpack package in R; Wolf & Universität Bielefeld 2012). Bagplots are the bivariate generalization of the well-known univariate boxplot, with the 50% most central data shown by a bag-shaped surface (Rousseeuw, Ruts & Tukey 1999).

Results

FUNCTIONAL RESPONSE

The frequency distribution of the durations of search bouts did not deviate from the exponential distribution (Fig. 3A; Cramér-von Mises test $\omega_n^2 = 1.93$; $n = 2{,}109$; $P = 1$). This was also the case for the distribution of handling times (Fig. 3B; $\omega_n^2 = 13.38$; $n = 1{,}242$; $P = 1$) and moving bouts (Fig. 3C; $\omega_n^2 = 2.90$; $n = 929$; $P = 1$).

Two models explaining inter-state transition rates were about equally plausible. The best model (AIC weight = 0.52) included all three main effects (the densities of *Dosinia*, *Loripes*, and red knots) and one interaction (between *Dosinia* and *Loripes* densities; Table 1). The second best model (AIC weight = 0.43), included *Dosinia* and red knot density only. All the other models were less supported ($\Delta AIC > 2$) and therefore considered unlikely.

280 In both of the plausible models, *Dosinia* density had positive effects on α, β and γ (Tables 2-3).
281 This means that at higher (available) *Dosinia* densities, red knots were: (1) more likely to resume
282 searching after having found and handled a prey (α); (2) more likely to shift to handling state while
283 searching, or stated more simply, found prey at a higher rate (β); and (3) returned to the searching state at
284 higher rates after having moved (γ). *Loripes* density had an effect on β, which can be seen by considering
285 the main effect and the interaction with *Dosinia* density (Table 2). Particularly, the main effect was
286 positive but non-significant and the interaction was negative (and significant). The results imply that prey
287 encounter rate β increased with *Loripes* density at low *Dosinia* density but showed no response to *Loripes*
288 density at higher *Dosinia* densities (also refer to model-averaged model fits in Fig. 4). Red knot density
289 affected transition rates α, μ, δ and γ. After handling prey in dense flocks, red knots were more likely to
290 start moving (positive effect on μ) and less likely to return to the searching state (negative effect on α).
291 Also when searching at high red knot densities they were more likely to give up searching and move on
292 (δ). In addition, once moving through dense flocks, red knots were less likely to get back into their
293 searching mode (γ).
294
295 RED KNOT DISTRIBUTION
296 The majority of the 5,666 individual red knots selected feeding sites that had higher available *Dosinia* and
297 available *Loripes* densities (Fig. 4: small dark grey bag) than average densities (Fig. 4: large light grey
298 bag based on kriged prey densities at benthos sites). Feeding sites contained higher densities of *Dosinia* (t
299 = 3.59, df = 233.5, P < 5e-4) and *Loripes* (t = 4.39, df = 234.7, P < 5e-05) than our benthos sampling sites
300 (again using kriged estimates, also at benthos sites). By feeding at relatively high prey densities, the red
301 knots obtained relatively high intake rates (solid lines in Fig. 4, which are interference-free intake rates as
302 predicted by the model-averaged multi-state model in which $\log_e$(red knot density) = 0).
303
304

Discussion

FUNCTIONAL RESPONSE

The Markov-chain modelling approach that we used has yielded important insights in the dynamical processes affecting prey intake rates and movements by red knots. We start with a discussion on the effects of conspecific density on foraging behaviour. The local density of red knots affected multiple behavioural transitions which determine the functional response. Although interference is often assumed to reduce searching efficiency directly (e.g. see citation classic by Hassell & Varley 1969), it was not observed in our study (no effect of conspecific density on β). Instead, the effects of interference appeared more subtle via a reduction of the transition rates *to* searching from handling (α) and moving (γ). Stated otherwise, the more conspecifics surround a given red knot, the smaller the likelihood that this bird would commence searching. The density of conspecifics in the vicinity increased the transition rates from handling to moving and from searching to moving (μ and δ, respectively). These conspecific density effects can be interpreted as movement behaviour to avoid or reduce possible direct interference effects, a phenomenon coined 'cryptic interference' (Gyimesi, Stillman & Nolet 2010; Bijleveld, Folmer & Piersma 2012).

Enter the effects of prey density. Starting with *Dosinia*, higher densities of this prey stimulated the transitions to searching, both when handling (α) and when moving (γ). These effects can be interpreted as behaviour leading to area-restricted search (Barraquand & Benhamou 2008) and would not have been detected if we had tested data against the more static classical functional response models (see below). *Dosinia* also had a positive effect on β. This effect is expected, since β, the transition rate between searching and handling, is equivalent to prey encounter rate (van der Meer & Smallegange 2009), which increases with prey density in any functional response model (Jeschke, Kopp & Tollrian 2002). It came as a surprise that the coefficient was smaller than one. A coefficient of one is expected under Holling's assumption of a searching efficiency that does not vary with prey density (refer to eqn. 8 in which β would then be a linear function of prey density and β_0 would be searching efficiency; also see discussion below). A coefficient smaller than one means reduced searching efficiencies at higher prey

densities, a phenomenon likely due to higher rates of 'invisible' prey rejection at higher prey densities (due to a digestive constraint red knots are expected to reject an increasing proportion of *Dosinia* at high densities; van Gils *et al.* 2013). As prey rejections may occur before prey are lifted to the sediment surface, we have likely missed prey rejections, thereby underestimating searching efficiency at higher prey densities.

Only at low prey densities did more *Loripes* increase intake rate (model fits in Fig. 4 and Table 2). In the light of our recent findings, this result did not surprise us. Although *Loripes* with its high flesh-to-shell ratios may seem the ideal prey, it is not. This is because an endosymbiosis with chemoautotrophic sulphur-oxidizing bacteria (van der Geest *et al.* 2014) makes *Loripes*, once ingested by red knots, mildly toxic (Oudman *et al.* 2014). Red knots suffer from diarrhoea when only eating *Loripes*, leading to dehydration and reduced feeding rates; the birds face this toxin constraint at available *Loripes* of at least 50 m^{-2} (dashed horizontal line Fig. 4 based on parameters in van Gils *et al.* 2013). Hence, below this critical *Loripes* density, intake rate should increase with both *Loripes* and *Dosinia* density, whereas above this critical *Loripes* density, red knots should reject an increasing proportion of *Loripes* and intake rates should level off with *Loripes* density and only increase with *Dosinia* (as stated above, also *Dosinia* will be rejected, but at a much lower rate). This is the key prediction of the recently published optimal diet model that takes account of *Loripes*' toxicity (TDRM; van Gils *et al.* 2013). As illustrated by the lines of equal intake rate predicted by the model-averaged multi-state model (Fig. 4), it corresponds nicely with the intake rates found in this study. These lines shift from being diagonal (i.e. more or less equal intake rate on *Dosinia* and *Loripes*) to vertical (i.e. additional increase in intake due to *Dosinia* only) when going from low to high *Loripes* densities in the environmental bagplot.

RED KNOT DISTRIBUTION

Red knots selected sites with relatively high densities of both *Dosinia* and *Loripes* (Fig. 4). That they selected for high *Loripes* densities may be surprising in the light of *Loripes*' toxicity effects. However, 2007 was a relatively poor year in terms of *Dosinia* densities, and red knots would not have been able to

survive without the inclusion of *Loripes* in their diet (van Gils *et al.* 2013). Indeed, dropping analyses showed that in 2007 red knots included both *Loripes* and *Dosinia* in their diet, for about 60% and 40% respectively (Onrust *et al.* 2013; van Gils *et al.* 2013). Combining these diet compositions with the fitted numerical intake rates (~0.025 s^{-1}) yields energy intake rates of 0.1 mg ash-free dry mass per second (taking species-specific energy values for 2007 from van Gils *et al.* 2013).

GENERAL IMPLICATIONS

Movement ecology is a rapidly expanding field in which landscape ecology, animal behaviour and statistical physics come together, empirically encouraged by the ongoing miniaturization of animal tracking devices at ever higher resolutions (Nathan *et al.* 2008; Giuggioli & Bartumeus 2010). Although optimal foraging theory may be considered as one of the theoretical backbones of this exciting scientific proliferation, we are yet at the infancy to link forager movement with processes affecting prey encounter rate. The functional response is the fundamental link between a forager's intake rate and its prey. It therefore makes perfect sense to integrate movement decisions with the two basic behavioural components underlying any functional response, i.e. searching and handling events. By doing so, movement processes have naturally emerged from our modelling exercise, i.e. area-restricted search (transition rates to/from movement affected by food density) and cryptic interference (transition rates to/from movement affected by competitor density). Without the explicit consideration of movement behaviour, these subtle foraging behaviours would probably not have been unveiled.

The flexible Markov chain modelling framework allowed us to explore what outcome we would have obtained if we had ignored the movement state in our models by setting covariate effects on transitions to (δ and μ) and from (γ and ε) movement to zero (i.e. still allowing for movement, but without allowing covariate effects on transitions to and from movement state). The results are striking (Tables S2-S4 in Supporting Information). Although the two most plausible models are still the same (albeit the order is reversed; Table S2), the effects of prey density in the full model become non-significant (Table S4). The only significant effect remaining is the negative effect of red knot density on α, the transition from

383 handling to searching (Table S4). Hence, by ignoring spatial movements, we would have overlooked the
384 subtle effects of *Loripes* density and its interaction with *Dosinia* density on red knot intake rate.
385 More subtlety is lost if we would, besides ignoring movement, stick to the rigid assumptions of
386 Holling's disc equation, namely that both searching efficiency and handling time are not affected by prey
387 density (Holling 1959; Piersma *et al.* 1995). In that case, the only plausible model remaining is the model
388 in which red knot density and the *summed* densities of *Dosinia* and *Loripes* feature (Tables S5-S6).
389 Hence, under these restricted parameter settings we would have concluded that prey density affects intake
390 rate, but we would not have detected the differential roles of *Dosinia* and *Loripes*.
391 Clearly, there are many benefits to include movement as a behavioural element. Similarly, adding
392 realistic and detailed consumer behaviour to movement analyses is of equally great value. Until now, one
393 of the pillars in movement ecology consisted of models featuring solitary, uninformed foragers (Sims *et*
394 *al.* 2008). In the real world however, foragers tend not to feed alone (Giraldeau & Caraco 2000) and
395 usually have basic information about food distributions in their environment (Olsson *et al.* 1999; van Gils
396 *et al.* 2006; Bijleveld *et al.* 2014). Therefore, foragers will tweak their movements in response to
397 encounters with conspecifics and food. Our work shows how real-world foragers do this. We hope that
398 our effort to integrate movement behaviour and consumer-resource theory adds realism to the exciting
399 fields of movement ecology and foraging theory.
400

401 ## Acknowledgements

402 We thank Parc National du Banc d'Arguin (PNBA) for their hospitality, the hosting of our presence and the
403 permission to work in and from the Iwik scientific station. Lemhaba ould Yarba made the logistic arrangements.
404 Joop van Eerbeek, Erik J. Jansen, Han Olff and El-Hacen Mohamed El-Hacen helped collecting and sorting benthos
405 samples. Valuable comments on the manuscript were given by Allert Bijleveld, Jaap van der Meer, Ola Olsson,
406 Thomas Oudman, Isabel M. Smallegange, an anonymous referee and by the 'literature club' of the Centre for
407 Integrative Ecology during JAvG's sabbatical at Deakin University. Dick Visser polished the figures. This work is

408 supported by an NWO WOTRO Integrated Programme grant (W.01.65.221.00) to TP, an NWO travel grant (R 84-
409 639) to EOF, and an NWO VIDI grant (864.09.002) to JAvG.

410

411 Data accessibility

412 Data is archived on Dryad digital archive, doi:10.5061/dryad.m9j80 (van Gils *et al.* 2014).

413

414 References

415 Abrams, P.A. (2014) Why ratio dependence is (still) a bad model of predation. *Biological Reviews,* **Early View**, doi:
416 10.1111/brv.12134.
417 Arditi, R. & Ginzburg, L.R. (2012) *How Species Interact: Altering the Standard View on Trophic Ecology*. Oxford
418 University Press, Oxford.
419 Avgar, T., Kuefler, D. & Fryxell, J.M. (2011) Linking rates of diffusion and consumption in relation to resources.
420 *American Naturalist,* **178**, 182-190.
421 Barraquand, F. & Benhamou, S. (2008) Animal movements in heterogeneous landscapes: identifying profitable
422 places and homogeneous movement bouts. *Ecology,* **89**, 3336-3348.
423 Beauchamp, G. (1998) The effect of group size on mean food intake rate in birds. *Biological Reviews,* **73**, 449-472.
424 Bijleveld, A.I., Folmer, E.O. & Piersma, T. (2012) Experimental evidence for cryptic interference among socially
425 foraging shorebirds. *Behavioral Ecology,* **23**, 806-814.
426 Bijleveld, A.I., van Gils, J.A., Jouta, J. & Piersma, T. (2014) Benefits of foraging in small groups: an experimental
427 study on public information use in red knots *Calidris canutus*. *Behavioural Processes,* **Early View**, doi:
428 10.1016/j.beproc.2014.1009.1003.
429 Burnham, K.P. & Anderson, D.R. (2002) *Model Selection and Multimodel Inference*. Springer, New York.
430 Chakraborty, A., Singh, M., Lucy, D. & Ridland, P. (2007) Predator–prey model with prey-taxis and diffusion.
431 *Mathematical and Computer Modelling,* **46**, 482-498.
432 Couzin, I.D., Krause, J., Franks, N.R. & Levin, S.A. (2005) Effective leadership and decision-making in animal
433 groups on the move. *Nature,* **433**, 513-516.

434 Elgar, M.A. (1989) Predator vigilance and group-size in mammals and birds - a critical review of the empirical
435 evidence. *Biological Reviews of the Cambridge Philosophical Society,* **64**, 13-33.
436 Fernández-Juricic, E., Siller, S. & Kacelnik, A. (2004) Flock density, social foraging, and scanning: an experiment
437 with starlings. *Behavioral Ecology,* **15**, 371-379.
438 Folmer, E.O., Olff, H. & Piersma, T. (2010) How well do food distributions predict spatial distributions of
439 shorebirds with different degrees of self-organization? *Journal of Animal Ecology,* **79**, 747-756.
440 Folmer, E.O., Olff, H. & Piersma, T. (2012) The spatial distribution of flocking foragers: disentangling the effects of
441 food availability, interference and conspecific attraction by means of spatial autoregressive modeling.
442 *Oikos,* **121**, 551-561.
443 Folmer, E.O., van der Geest, M., Jansen, E., Olff, H., Anderson, T.M., Piersma, T. & van Gils, J.A. (2012) Seagrass-
444 sediment feedback: an exploration using a non-recursive structural equation model. *Ecosystems,* **15**, 1380-
445 1393.
446 Fryxell, J.M., Hazell, M., Börger, L., Dalziel, B.D., Haydon, D.T., Morales, J.M., McIntosh, T. & Rosatte, R.C.
447 (2008) Multiple movement modes by large herbivores at multiple spatiotemporal scales. *Proceedings of the*
448 *National Academy of Sciences,* **105**, 19114-19119.
449 Giraldeau, L.-A. & Caraco, T. (2000) *Social Foraging Theory*. Princeton University Press, Princeton, New Jersey.
450 Giuggioli, L. & Bartumeus, F. (2010) Animal movement, search strategies and behavioural ecology: a cross-
451 disciplinary way forward. *Journal of Animal Ecology,* **79**, 906-909.
452 Gurarie, E. & Ovaskainen, O. (2013) Towards a general formalization of encounter rates in ecology. *Theoretical*
453 *Ecology,* **6**, 189-202.
454 Gyimesi, A., Stillman, R.A. & Nolet, B.A. (2010) Cryptic interference competition in swans foraging on cryptic
455 prey. *Animal Behaviour,* **80**, 791-797.
456 Hassell, M.P. & Varley, G.C. (1969) New inductive population model for insect parasites and its bearing on
457 biological control. *Nature,* **223**, 1133-1137.
458 Hiemstra, P.H., Pebesma, E.J., Twenhofel, C.J.W. & Heuvelink, G.B.M. (2008) Real-time automatic interpolation of
459 ambient gamma dose rates from the Dutch Radioactivity Monitoring Network. *Computers & Geosciences,*
460 **35**, 1711-1721.

461 Holling, C.S. (1959) Some characteristics of simple types of predation and parasitism. *Canadian Entomologist,* **91**,
462 385-398.
463 Honkoop, P.J.C., Berghuis, E.M., Holthuijsen, S., Lavaleye, M.S.S. & Piersma, T. (2008) Molluscan assemblages of
464 seagrass-covered and bare intertidal flats on the Banc d'Arguin, Mauritania, in relation to characteristics of
465 sediment and organic matter. *Journal of Sea Research,* **60**, 255-263.
466 Jackson, C.H. (2011) Multi-state models for panel data: the msm package for R. *Journal of Statistical Software,* **38**,
467 1-29.
468 Jeschke, J.M., Kopp, M. & Tollrian, R. (2002) Predator functional responses: discriminating between handling and
469 digesting prey. *Ecological Monographs,* **72**, 95-112.
470 Kriegler, F.J., Malila, W.A., Nalepka, R.F. & Richardson, W. (1969) Preprocessing transformations and their effects
471 on multispectral recognition. *Proceedings of the Sixth International Symposium on Remote Sensing of*
472 *Environment*, pp. 97-131.
473 Leyrer, J., Lok, T., Brugge, M., Dekinga, A., Spaans, B., van Gils, J.A., Sandercock, B.K. & Piersma, T. (2012)
474 Small-scale demographic structure suggests preemptive behavior in a flocking shorebird. *Behavioral*
475 *Ecology,* **23**, 1226-1233.
476 Marshall, G. & Jones, R.H. (1995) Multi-state Markov models and diabetic retinopathy. *Statistics in Medicine,* **14**,
477 1975-1983.
478 Nathan, R., Getz, W.M., Revilla, E., Holyoak, M., Kadmon, R., Saltz, D. & Smouse, P.E. (2008) A movement
479 ecology paradigm for unifying organismal movement research. *Proceedings of the National Academy of*
480 *Sciences,* **105**, 19052-19059.
481 Olsson, O., Wiktander, U., Holmgren, N.M.A. & Nilsson, S. (1999) Gaining ecological information about Bayesian
482 foragers through their behaviour. II. A field test with woodpeckers. *Oikos,* **87**, 264-276.
483 Onrust, J., de Fouw, J., Oudman, T., van der Geest, M., Piersma, T. & van Gils, J.A. (2013) Red Knot diet
484 reconstruction revisited: context dependence revealed by experiments at Banc d'Arguin, Mauritania. *Bird*
485 *Study,* **60**, 298-307.
486 Ottoni, E.B. (2000) EthoLog 2.2 - a tool for the transcription and timing of behavior observation sessions. *Behavior*
487 *Research Methods, Instruments & Computers,* **32**, 446-449.

488 Oudman, T., Onrust, J., de Fouw, J., Spaans, B., Piersma, T. & van Gils, J.A. (2014) Digestive capacity and toxicity
489 cause mixed diets in red knots that maximize energy intake rate. *American Naturalist,* **183**, 650-659.
490 Owen-Smith, N., Fryxell, J. & Merrill, E. (2010) Foraging theory upscaled: the behavioural ecology of herbivore
491 movement. *Philosophical Transactions of the Royal Society B: Biological Sciences,* **365**, 2267-2278.
492 Pebesma, E.J. (2004) Multivariable geostatistics in S: the gstat package. *Computers & Geosciences,* **30**, 683-691.
493 Piersma, T. (2012) What is habitat quality? Dissecting a research portfolio on shorebirds. *Birds and Habitat:*
494 *Relationships in Changing Landscapes* (ed. R.J. Fuller), pp. 383-407. Cambridge University Press.
495 Piersma, T., van Gils, J., de Goeij, P. & van der Meer, J. (1995) Holling's functional response model as a tool to link
496 the food-finding mechanism of a probing shorebird with its spatial distribution. *Journal of Animal Ecology,*
497 **64**, 493-504.
498 Piersma, T. & van Gils, J.A. (2011) *The Flexible Phenotype: A Body-Centred Integration of Ecology, Physiology*
499 *and Behaviour*. Oxford University Press, Oxford.
500 Pusev, R. & Yakovlev, M. (2011) exptest: Tests for Exponentiality. R package version 1.0. http://CRAN.R-
501 project.org/package=exptest.
502 R Core Team (2013) *R: A language and environment for statistical computing*. R Foundation for Statistical
503 Computing, Vienna, Austria.
504 Rousseeuw, P.J., Ruts, I. & Tukey, J.W. (1999) The bagplot: A bivariate boxplot. *American Statistician,* **53**, 382-
505 387.
506 Sims, D.W., Southall, E.J., Humphries, N.E., Hays, G.C., Bradshaw, C.J.A., Pitchford, J.W., James, A., Ahmed,
507 M.Z., Brierley, A.S., Hindell, M.A., Morritt, D., Musyl, M.K., Righton, D., Shepard, E.L.C., Wearmouth,
508 V.J., Wilson, R.P., Witt, M.J. & Metcalfe, J.D. (2008) Scaling laws of marine predator search behaviour.
509 *Nature,* **451**, 1098-1103.
510 Smallegange, I.M. & van der Meer, J. (2010) Testing a stochastic version of the Beddington-DeAngelis functional
511 response in foraging shore crabs. *Marine Biology,* **157**, 1027-1040.
512 Stillman, R.A., Caldow, R.W.G., Goss-Custard, J.D. & Alexander, M.J. (2000) Individual variation in intake rate:
513 the relative importance of foraging efficiency. *Journal of Animal Ecology,* **69**, 484-493.
514 Stillman, R.A., Goss-Custard, J.D. & Caldow, R.W.G. (1997) Modelling interference from basic foraging behaviour.
515 *Journal of Animal Ecology,* **66**, 692-703.

Tinbergen, N., Impekoven, M. & Franck, D. (1967) An experiment on spacing out as a defence against predation. *Behaviour,* **28**, 307-320.

van den Hout, P.J., van Gils, J.A., Robin, F., van der Geest, M., Dekinga, A. & Piersma, T. (2014) Interference from adults forces young red knots to forage longer and in dangerous places. *Animal Behaviour,* **88**, 137-146.

van der Geest, M., Sall, A.A., Ely, S.O., Nauta, R.W., van Gils, J.A. & Piersma, T. (2014) Nutritional and reproductive strategies in a chemosymbiotic bivalve living in a tropical intertidal seagrass bed. *Marine Ecology Progress Series,* **501**, 113-126.

van der Heide, T., Govers, L.L., de Fouw, J., Olff, H., van der Geest, M., van Katwijk, M.M., Piersma, T., van de Koppel, J., Silliman, B.R., Smolders, A.J.P. & van Gils, J.A. (2012) A three-stage symbiosis forms the foundation of seagrass ecosystems. *Science,* **336**, 1432-1434.

van der Meer, J. & Ens, B.J. (1997) Models of interference and their consequences for the spatial distribution of ideal and free predators. *Journal of Animal Ecology,* **66**, 846-858.

van der Meer, J. & Smallegange, I.M. (2009) A stochastic version of the Beddington-DeAngelis functional response: modelling interference for a finite number of predators. *Journal of Animal Ecology,* **78**, 134-142.

van Gils, J.A. (2010) State-dependent Bayesian foraging on spatially autocorrelated food distributions. *Oikos,* **119**, 237-244.

van Gils, J.A., Spaans, B., Dekinga, A. & Piersma, T. (2006) Foraging in a tidally structured environment by red knots (*Calidris canutus*): ideal, but not free. *Ecology,* **87**, 1189-1202.

van Gils, J.A., van der Geest, M., Jansen, E.J., Govers, L.L., de Fouw, J. & Piersma, T. (2012) Trophic cascade induced by molluscivore predator alters pore-water biogeochemistry via competitive release of prey. *Ecology,* **93**, 1143-1152.

van Gils, J.A., van der Geest, M., Leyrer, J., Oudman, T., Lok, T., Onrust, J., de Fouw, J., van der Heide, T., van den Hout, P.J., Spaans, B., Dekinga, A., Brugge, M. & Piersma, T. (2013) Toxin constraint explains diet choice, survival and population dynamics in a molluscivore shorebird. *Proceedings of the Royal Society B: Biological Sciences,* **280**, 20130861.

Wiersma, P. & Piersma, T. (1994) Effects of microhabitat, flocking, climate and migratory goal on energy expenditure in the annual cycle of red knots. *Condor,* **96**, 257-279.

543 Wolf, P. & Universität Bielefeld (2012) aplpack: another plot PACKage: stem.leaf, bagplot, faces, spin3R, and some
544 slider functions. R package version 1.2.7. http://CRAN.R-project.org/package=aplpack.
545 Wolff, W.J. & Smit, C. (1990) The Banc d'Arguin, Mauritania, as an environment for coastal birds. *Ardea,* **78**, 17-
546 38.
547 Zwarts, L. & Blomert, A.-M. (1992) Why knots *Calidris canutus* take medium-sized *Macoma balthica* when six
548 prey species are available. *Marine Ecology - Progress Series,* **83**, 113-128.

549

550

551 **Table 1.** Akaike's Information Criteria (AIC) of the fitted multi-state models explaining transition rates
552 between S, H and M on the basis of all possible combinations of the explanatory variables, including their
553 two-way interactions ($D = \log_e$(*Dosinia* available density); $L = \log_e$(*Loripes* available density); $DL =$
554 $\log_e$(available densities *Dosinia* plus *Loripes*); $K = \log_e$(red knot density)). The best models with ΔAIC <
555 2 are given in bold. The best model's AIC given below the table; np denotes the number of model
556 parameters.

Model	Np	ΔAIC	AIC weight
constant + *D* + *L* + *K* + *D*:*L*	**25**	**0.00**	**0.52**
constant + *D* + *K*	**15**	**0.37**	**0.43**
constant + *D* + *L* + *K*	20	4.64	0.05
constant + *D* + *K* + *D*:*K*	20	9.58	0.00
constant + *D* + *L* + *K* + *D*:*K*	25	13.57	0.00
constant + *D* + *L* + *K* + *D*:*L* + *L*:*K*	30	15.04	0.00
constant + *D* + *L* + *K* + *D*:*L* + *D*:*K*	30	20.54	0.00
constant + *K*	10	22.86	0.00
constant + *D* + *L* + *K* + *L*:*K*	25	24.37	0.00
constant + *DL* + *K*	15	28.17	0.00
constant + *D* + *L* + *K* + *D*:*K* + *L*:*K*	30	28.45	0.00
constant + *L* + *K*	15	35.22	0.00
constant + *DL* + *K* + *DL*:*K*	20	36.81	0.00
constant + *L* + *K* + *L*:*K*	20	37.36	0.00
constant + *D*	10	45.04	0.00
constant + *D* + *L* + *K* + *D*:*L* + *D*:*K* + *L*:*K*	35	46.24	0.00
constant + *D* + *L*	15	55.67	0.00
constant + *D* + *L* + *D*:*L*	20	58.28	0.00
constant + *D* + *L* + *K* + *D*:*L* + *D*:*K* + *L*:*K* + *D*:*L*:*K*	40	58.99	0.00
constant	5	67.76	0.00
constant + *L*	10	71.08	0.00
constant + *DL*	10	73.63	0.00

557 AIC = 26,862.97

Table 2. Regression coefficients of the best multi-state model (i.e. upper model in Table 1), describing transition rates (s^{-1}) between handling (H), searching (S) and moving (M; with 95% c.i. given in brackets). Note that rows in baseline matrix sum to zero, with diagonal entries giving the negative of a state's mean transition rate (i.e. mean bout length = 1 / mean transition rate). Significant covariate effects are given in bold.

Baseline transition rates (with covariates set to 0):

From:	To: H	S	M
H	-0.404 (-0.603, -0.271)	0.389 (0.258, 0.585)	0.015 (0.003, 0.091)
S	0.024 (0.016, 0.037)	-0.046 (-0.064, -0.034)	0.022 (0.014, 0.036)
M	0	0.375 (0.240, 0.586)	-0.375 (-0.586, -0.240)

Log-linear effects of $\log_e$(*Dosinia* density):

From:	To: H	S	M
H	0	**0.365 (0.070, 0.659)**	-0.043 (-1.363, 1.276)
S	**0.372 (0.074, 0.671)**	0	-0.032 (-0.392, 0.327)
M	0	**0.426 (0.082, 0.770)**	0

Log-linear effects of $\log_e$(*Loripes* density):

From:	To: H	S	M
H	0	0.098 (-0.108, 0.303)	0.035 (-0.838, 0.907)
S	0.151 (-0.054, 0.355)	0	-0.020 (-0.258, 0.217)
M	0	0.054 (-0.166, 0.275)	0

Log-linear effects of $\log_e$(red knot density):

From:	To: H	S	M
H	0	**-0.099 (-0.150, -0.048)**	**0.370 (0.181, 0.560)**
S	0.004 (-0.047, 0.055)	0	**0.132 (0.075, 0.190)**
M	0	**-0.128 (-0.183, -0.072)**	0

Log-linear effects of $\log_e$(*Dosinia* density):$\log_e$(*Loripes* density) interaction:

From:	To: H	S	M
H	0	-0.061 (-0.225, 0.104)	-0.075 (-0.805, 0.656)
S	**-0.182 (-0.348, -0.015)**	0	-0.024 (-0.224, 0.176)
M	0	-0.108 (-0.300, 0.084)	0

572 **Table 3.** Regression coefficients of the second best multi-state model (i.e. second model in Table 1),
573 describing transition rates (s^{-1}) between handling (H), searching (S) and moving (M; with 95% c.i. given
574 in brackets). Significant covariate effects are given in bold.

575 Baseline transition rates (with covariates set to 0):

From:	To: H	S	M
H	-0.491 (-0.571, -0.422)	0.467 (0.399, 0.545)	0.024 (0.012, 0.048)
S	0.030 (0.026, 0.035)	-0.051 (-0.057, -0.045)	0.020 (0.017, 0.024)
M	0	0.395 (0.330, 0.474)	-0.395 (-0.474, -0.330)

576

577 Log-linear effects of $\log_e$(*Dosinia* density):

From:	To: H	S	M
H	0	**0.207 (0.077, 0.337)**	-0.306 (-0.878, 0.265)
S	**0.129 (0.000, 0.258)**	0	0.045 (-0.109, 0.199)
M	0	**0.254 (0.094, 0.413)**	0

578

579 Log-linear effects of $\log_e$(red knot density):

From:	To: H	S	M
H	0	**-0.064 (-0.113, -0.015)**	**0.265 (0.082, 0.448)**
S	0.012 (-0.037, 0.061)	0	**0.108 (0.051, 0.164)**
M	0	**-0.102 (-0.156, -0.048)**	0

580

581 **Fig. 1.** Red knots show three behavioural states (searching S; handling H; moving M), between which
582 they alternate while foraging (Greek symbols indicate transition rates). Note that the transition from
583 moving to handling does not exist, i.e. handling is always preceded by searching.

584

585 **Fig. 2.** (A) Map of our study area around the Iwik village (19º53' N; 16º18' W), showing observation
586 towers A-I and the observation area around each of them. Colours represent the NDVI and are indicative
587 of seagrass coverage (based on a Landsat 5 image taken at 21 August 2007). Light grey shading indicates
588 the mainland, darker grey represents the sea. (B) Around each tower, exemplified here for tower D, an
589 annulus was divided into 128 'bird sections' (bordered by thin lines) and 16 'benthos sections' for
590 stratification (bordered by thick lines); each benthos section had two randomly located benthos stations
591 (labelled dots), with two benthos samples taken at each station.

592

593 **Fig. 3.** Frequency distributions of the durations (s) of the three behavioural states: searching, handling,
594 and moving. Each frequency distribution complies with the exponential distribution, with lines giving
595 maximum-likelihood fits (yielding mean ± SD rates of 0.059 ± 0.001 s^{-1} for searching; 0.552 ± 0.016 s^{-1}
596 for handling; 0.424 ± 0.014 s^{-1} for moving).

597

598 **Fig. 4.** State space of the available *Loripes* densities against available *Dosinia* densities in 2007 in the
599 environment (larger light grey 'bag') and at the sites selected by individual red knots (smaller dark grey
600 'bag'). These bagplots include the most central half of the data. Letters indicate the average prey densities
601 at the knot-selected sites for each tower, with the size of the letter indicative for the number of
602 individuals. Three curved lines are lines of equal intake rate (s^{-1}) as predicted by the model-averaged
603 multi-state model (these are interference-free intake rates by setting red knot density to 1). Dashed

604 horizontal line gives minimal *Loripes* density at which red knots face their toxin constraint (see
605 Discussion).

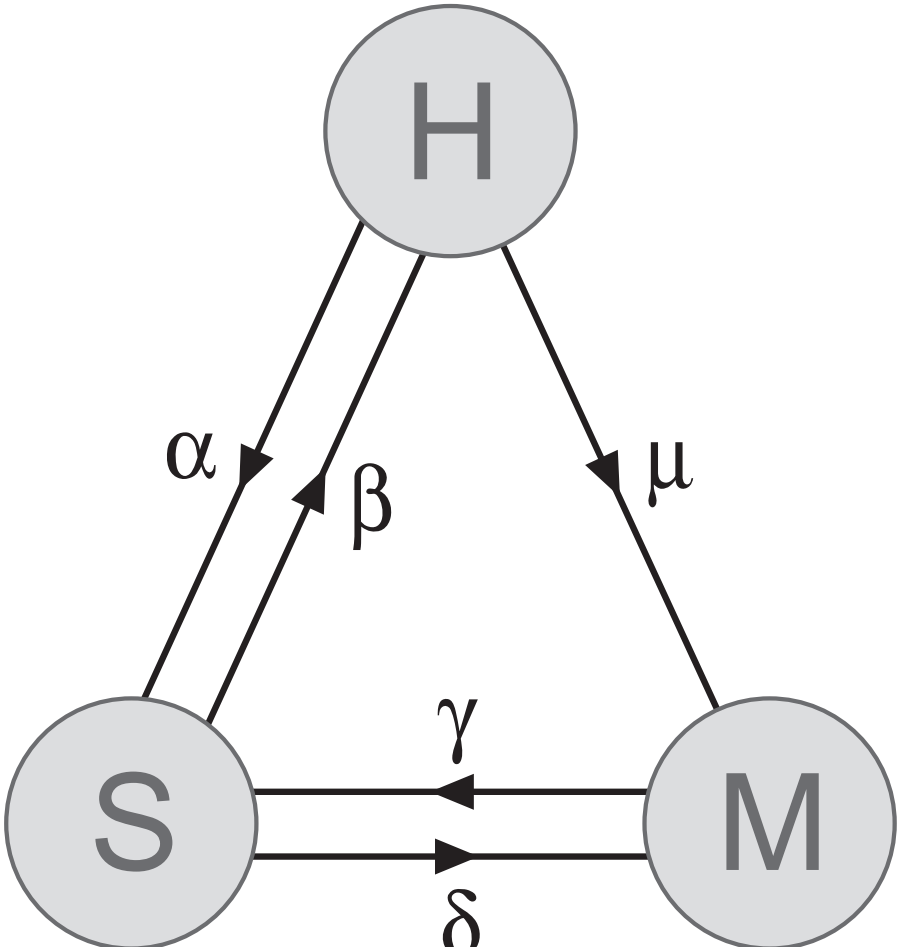
H
α
β
μ
γ
S
M
δ

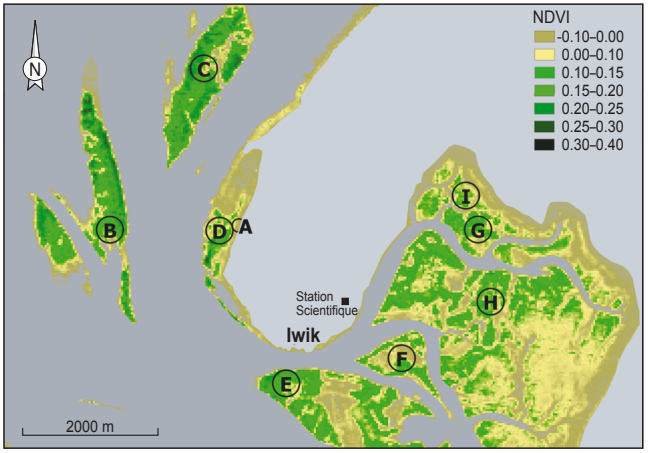
N
NDVI
-0.10–0.00
0.00–0.10
0.10–0.15
0.15–0.20
0.20–0.25
0.25–0.30
0.30–0.40
A
B
C
D
E
F
G
H
I
Station
Scientifique
Iwik
2000 m

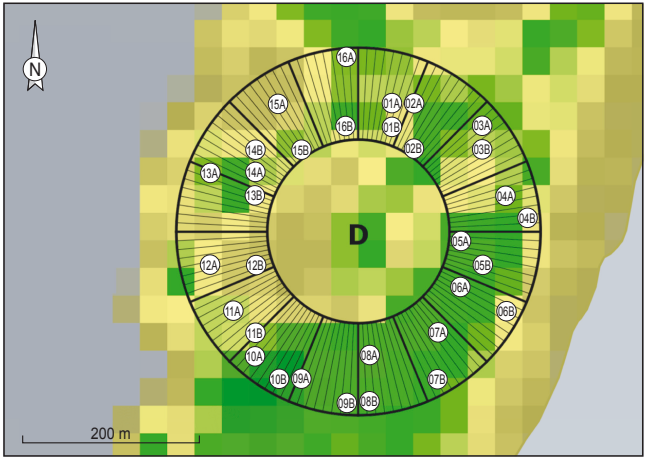
N
D
16A
01A
02A
03A
03B
04A
04B
05A
05B
06A
06B
07A
07B
08A
08B
09A
09B
10A
10B
11A
11B
12A
12B
13A
13B
14A
14B
15A
15B
16B
01B
02B
200 m

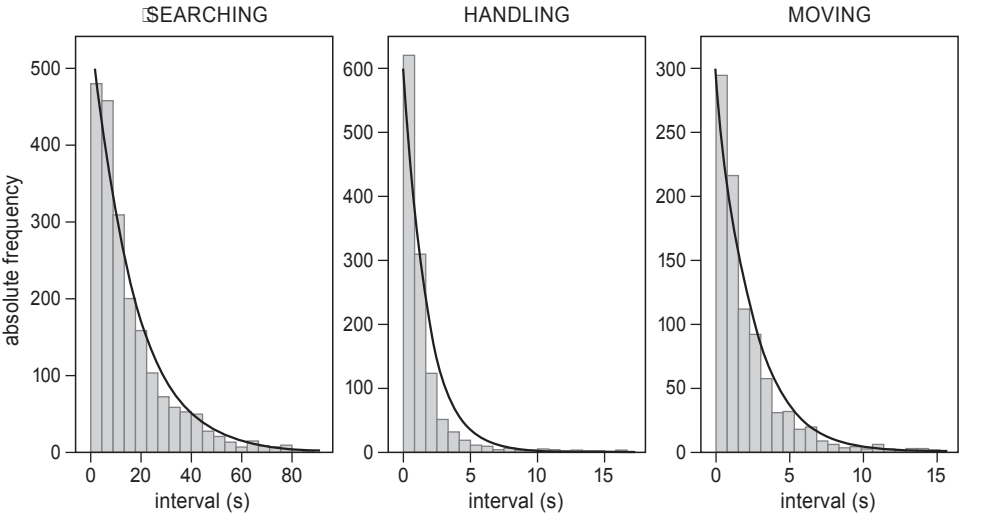
SEARCHING
HANDLING
MOVING
absolute frequency
interval (s)
interval (s)
interval (s)
0
100
200
300
400
500
600
50
150
250
0
20
40
60
80
5
10
15

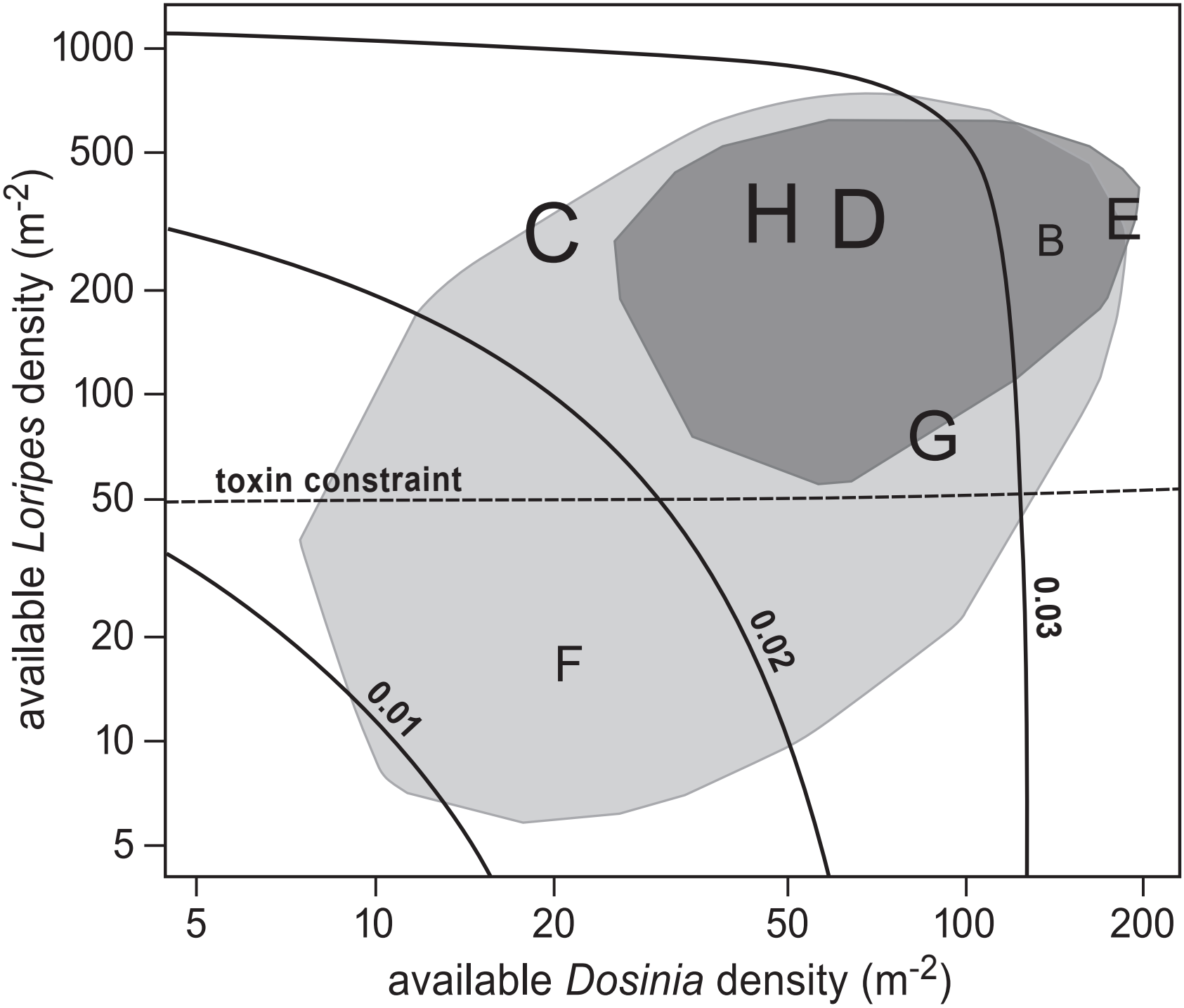
1000
500
200
100
50
20
10
5
available *Loripes* density (m^{-2})
toxin constraint
C
H
D
B
E
G
F
0.01
0.02
0.03
5
10
20
50
100
200
available *Dosinia* density (m^{-2})

[Supporting Information:]

Table S1. ΔAIC derived from regressions used for universal kriging of prey densities. All combinations of NDVI and $NDVI^2$ were used as auxiliary predictors and the regression model yielding the lowest AIC was selected for kriging (i.e. ΔAIC = 0). Prey densities were modelled separately for year (2007, 2008), species (*Dosinia*, *Loripes*) and tower (A-I; columns).

***Dosinia* (2007)**	**A**	**B**	**C**	**D**	**E**	**F**	**G**	**H**	**I**
constant	-	10.03	2.38	0.00	0.00	2.16	0.00	0.10	-
constant+NDVI	-	2.48	4.31	1.57	1.85	1.32	0.38	0.00	-
constant+$NDVI^2$	-	7.19	4.31	1.16	1.87	0.00	0.63	0.03	-
constant+NDVI+$NDVI^2$	-	0.00	0.00	2.01	3.80	0.92	2.08	1.99	-

***Loripes* (2007)**	**A**	**B**	**C**	**D**	**E**	**F**	**G**	**H**	**I**
constant	-	14.46	11.80	15.52	23.91	55.25	14.47	13.44	-
constant+NDVI	-	1.78	1.88	10.15	0.15	21.80	0.00	2.73	-
constant+$NDVI^2$	-	0.00	0.00	5.86	0.00	4.29	1.09	6.45	-
constant+NDVI+$NDVI^2$	-	1.96	1.64	0.00	1.86	0.00	1.81	0.00	-

***Dosinia* (2008)**	**A**	**B**	**C**	**D**	**E**	**F**	**G**	**H**	**I**
constant	21.03	-	-	0.74	-	-	-	-	0.00
constant+NDVI	0.00	-	-	0.01	-	-	-	-	1.76
constant+$NDVI^2$	1.41	-	-	0.00	-	-	-	-	1.30
constant+NDVI+$NDVI^2$	1.39	-	-	1.97	-	-	-	-	2.40

***Loripes* (2008)**	**A**	**B**	**C**	**D**	**E**	**F**	**G**	**H**	**I**
constant	11.73	-	-	32.58	-	-	-	-	11.04
constant+NDVI	0.74	-	-	0.00	-	-	-	-	0.00
constant+$NDVI^2$	5.11	-	-	3.46	-	-	-	-	2.79
constant+NDVI+$NDVI^2$	0.00	-	-	1.79	-	-	-	-	1.65

Table S2. Ranking of multi-state models in which covariate effects on transitions to and from the movement state are set to zero. Covariates defined as before. The most plausible models with ΔAIC < 2 are given in bold, with the best model's AIC given below the table; np denotes the number of parameters.

Model	Np	ΔAIC	AIC weight
constant + *D* + *K*	**9**	**0.00**	**0.38**
constant + *D* + *L* + *K* + *D:L*	**13**	**0.87**	**0.25**
constant + *D* + *L* + *K*	11	2.37	0.12
constant + *D* + *K* + *D*:*K*	11	3.10	0.08
constant + *D* + *L* + *K* + *D*:*L* + *D*:*K*	15	3.56	0.06
constant + *D* + *L* + *K* + *D*:*L* + *D*:*K* + *L*:*K* + *D*:*L*:*K*	19	5.11	0.03
constant + *D* + *L* + *K* + *D*:*K*	13	5.90	0.02
constant + *D* + *L* + *D:L*	11	6.05	0.02
constant + *D*	7	6.39	0.02
constant + *D* + *L* + *K* + *L*:*K*	13	8.29	0.01
constant + *D* + *L* + *K* + *D*:*K* + *L*:*K*	15	9.26	0.00
constant + *D* + *L*	9	9.43	0.00
constant + *D* + *L* + *K* + *D:L* + *L:K*	15	9.91	0.00
constant + *DL* + *K*	9	13.13	0.00
constant + *D* + *L* + *K* + *D*:*L* + *D*:*K* + *L*:*K*	17	13.93	0.00
constant + *K*	7	14.18	0.00
constant + *DL* + *K* + *DL:K*	11	14.30	0.00
constant + *L* + *K*	9	18.24	0.00
constant	5	20.91	0.00
constant + *DL*	7	21.31	0.00
constant + *L* + *K* + *L:K*	11	21.98	0.00
constant + *L*	7	22.91	0.00

AIC = 26,909.82

Table S3. Regression coefficients of the most plausible multi-state model (i.e. upper model in Table S2), in which covariate effects on transitions to and from the movement state are set to zero (with 95% c.i. given in brackets). Significant covariate effects are given in bold.

Baseline transition rates (with covariates set to 0):

From:	To: H	S	M
H	-0.496 (-0.575, -0.428)	0.469 (0.401, 0.547)	0.028 (0.021, 0.035)
S	0.029 (0.025, 0.034)	-0.054 (-0.059, -0.049)	0.024 (0.023, 0.026)
M	0	0.424 (0.397, 0.452)	-0.424 (-0.452, -0.397)

Log-linear effects of $\log_e$(*Dosinia* density):

From:	To: H	S	M
H	0	**0.230 (0.101, 0.360)**	0
S	**0.157 (0.027, 0.286)**	0	0
M	0	0	0

Log-linear effects of $\log_e$(red knot density):

From:	To: H	S	M
H	0	**-0.080 (-0.129, -0.030)**	0
S	0.008 (-0.042, 0.057)	0	0
M	0	0	0

Table S4. Regression coefficients of the second most plausible multi-state model (i.e. second model in Table S2), in which covariate effects on transitions to and from the movement state are set to zero (with 95% c.i. given in brackets). Significant covariate effects are given in bold.

Baseline transition rates (with covariates set to 0):

From:	To: H	S	M
H	-0.466 (-0.683, -0.318)	0.441 (0.295, 0.661)	0.024 (0.019, 0.032)
S	0.026 (0.017, 0.039)	-0.050 (-0.063, -0.041)	0.024 (0.023, 0.026)
M	0	0.426 (0.400, 0.455)	-0.426 (-0.455, -0.400)

Log-linear effects of $\log_e$(*Dosinia* density):

From:	To: H	S	M
H	0	0.228 (-0.067, 0.522)	0
S	0.258 (-0.044, 0.561)	0	0
M	0	0	0

Log-linear effects of $\log_e$(*Loripes* density):

From:	To: H	S	M
H	0	0.044 (-0.159, 0.247)	0
S	0.116 (-0.088, 0.321)	0	0
M	0	0	0

Log-linear effects of $\log_e$(red knot density):

From:	To: H	S	M
H	0	**-0.076 (-0.126, -0.026)**	0
S	-0.002 (-0.054, 0.050)	0	0
M	0	0	0

Log-linear effects of $\log_e$(*Dosinia* density):$\log_e$(*Loripes* density) interaction:

From:	To: H	S	M
H	0	-0.009 (-0.174, 0.155)	0
S	-0.122 (-0.291, 0.046)	0	0
M	0	0	0

Table S5. Ranking of multi-state models in which covariate effects on transitions to and from the movement state are set to zero *and* in which Holling's assumptions about constancy of searching efficiency and handling time are fulfilled. Therefore, models that do not include prey density or that include prey density interactions are excluded. Covariates as defined as before ($D = \log_e$(*Dosinia* available density); $L = \log_e$(*Loripes* available density); $DL = \log_e$(available densities *Dosinia* plus *Loripes*); $K = \log_e$(red knot density)). The most plausible models with ΔAIC < 2 are given in bold, with the best model's AIC given below the table; np denotes the number of parameters.

Model	**np**	**ΔAIC**	**AIC weight**
constant + *DL* + *K*	**7**	**0.00**	**0.88**
constant + *D* + *K*	7	4.07	0.11
constant + *D*	5	10.80	0.00
constant + *DL*	5	15.41	0.00
constant + *D* + *L* + *K*	7	189.03	0.00
constant + *D* + *L*	5	212.12	0.00
constant + *L* + *K*	7	350.39	0.00
constant + *L*	5	370.07	0.00

AIC = 27,080.08

Table S6. Regression coefficients of the most plausible multi-state model (i.e. upper model in Table S5), in which covariate effects on transitions to and from the movement state are set to zero *and* in which Holling's assumptions on a constant searching efficiency and a constant handling time are fulfilled (with 95% c.i. given in brackets). Significant covariate effects are given in bold.

Baseline transition rates (with covariates set to 0):

From:	To: H	S	M
H	-0.615 (-0.669, -0.566)	0.588 (0.539, 0.641)	0.027 (0.021, 0.035)
S	0.005 (0.004, 0.005)	-0.029 (-0.031, -0.027)	0.024 (0.023, 0.026)
M	0	0.424 (0.397, 0.452)	-0.424 (-0.452, -0.397)

Log-linear effects of $\log_e$(*Dosinia*+*Loripes* density):

From:	To: H	S	M
H	0	0	0
S	1	0	0
M	0	0	0

Log-linear effects of $\log_e$(red knot density):

From:	To: H	S	M
H	0	**-0.081 (-0.130, -0.032)**	0
S	**-0.074 (-0.122, -0.025)**	0	0
M	0	0	0